VILNIUS UNIVERSITY
CENTER FOR PHYSICAL SCIENCES AND TECHNOLOGY

Karolis Viskontas

FABRICATION AND CHARACTERIZATION OF LOW-DIMENSIONAL NANOMATERIAL SATURABLE ABSORBERS FOR MODE-LOCKING OF FIBER LASERS

Summary of doctoral thesis,
Technological Sciences, Material Engineering (08T)

Vilnius, 2016

Dissertation was prepared in 2011-2016 at the Center for Physical Sciences and Technology (CPST), and at the company EKSPLA. Part of the experiments was done at Tampere University of Technology (Finland).

Scientific supervisor:
Dr. Kęstutis Regelskis (*Center for Physical Sciences and Technology*, Technology Sciences, Material Engineering - 08T).
Scientific advisor:
Dr. Nerijus Rusteika (*Center for Physical Sciences and Technology*, Technology Sciences, Material Engineering - 08T).

Doctoral thesis will be defended at the Center for Physical Sciences and Technology in the senate of Physical Sciences:

Chairman:
Prof. habil. dr. Valerijus Smilgevičius (*Vilnius University*, Technology Sciences, Material Engineering - 08T).

Members:

1. Dr. Arūnas Varanavičius (*Vilnius University*, Physical Sciences, Physics - 02P);

2. Dr. Ramūnas Adomavičius (*Center for Physical Sciences and Technology*, Technology Sciences, Material Engineering - 08T);

3. Dr. Šarūnas Meškinis (*Kaunas University of Technology*, Technology Sciences, Material Engineering - 08T);

4. Prof. Dr. Almantas Galvanauskas (*University of Michigan (USA)*, Technology Sciences, Material Engineering - 08T);

This thesis will be under open consideration on 22nd of September, 2016 10 a.m. at the hall of CPST Institute of Physics.

Address: Savanoriu ave. 231, LT-02300 Vilnius, Lithuania.

Summary of doctoral thesis was distributed on 19th of September, 2016.

Doctoral thesis is available at the library of Vilnius University and accessible by link www.vu.lt/lt/naujienos/ivykiu-kalendorius

VILNIAUS UNIVERSITETAS
FIZINIŲ IR TECHNOLOGIJOS MOKSLŲ CENTRAS

Karolis Viskontas

NANOSTRUKTŪRINIŲ DARINIŲ, SKIRTŲ SKAIDULINIŲ LAZERIŲ MODŲ SINCHRONIZACIJAI, FORMAVIMAS IR PRITAIKYMAS, ELIMINUOJANT LAISVOS ERDVĖS ELEMENTUS

Daktaro disertacija santrauka,
Technologijos mokslai, medžiagų inžinerija (08T)

Vilnius, 2016

Disertacija rengta 2011-2016 metais Fizinių ir technologijos mokslų centro lazerinių technologijų skyriuje ir UAB „EKSPLA“ įmonėje. Dalis eksperimentų buvo atlikta Tamperės technologijos universitete (TUT, Tamperė, Suomija).

Mokslinis vadovas:

Dr. Kęstutis Regelskis (*Fizinių ir technologijos mokslų centras*, technologijos mokslai, medžiagų inžinerija -08T).

Konsultantas:

Dr. Nerijus Rusteika (*Fizinių ir technologijos mokslų centras*, technologijos mokslai, medžiagų inžinerija -08T).

Disertacija ginama Vilniaus Universiteto Medžiagų inžinerijos krypties taryboje:

Pirmininkas:
Prof. habil. dr. Valerijus Smilgevičius (*Vilniaus universitetas*, technologijos mokslai, medžiagų inžinerija – 08T)

Nariai:

1. Dr. Arūnas Varanavičius (*Vilniaus universitetas*, fiziniai mokslai, fizika - 02P);

2. Dr. Ramūnas Adomavičius (*Fizinių ir technologijos mokslų centras*, technologijos mokslai, medžiagų inžinerija – 08T);

3. Dr. Šarūnas Meškinis (*Kauno technologijos universitetas*, technologijos mokslai, medžiagų inžinerija – 08T);

4. Prof. dr. Almantas Galvanauskas (*Mičigano universitetas (JAV)*, technologijos mokslai, medžiagų inžinerija – 08T);

Disertacija bus ginama viešame Medžiagų inžinerijos krypties tarybos posėdyje 2016m. rugsėjo mėn. 22 d. 10 val. FMTC Fizikos instituto salėje.

Adresas: Savanorių pr. 231, LT-02300 Vilnius, Lietuva.

Disertacijos santrauka išsiuntinėta 2016 metų rugpjūčio mėn. 19 d.

Disertaciją galima peržiūrėti Vilniaus universiteto bibliotekoje ir VU interneto svetainėje adresu: www.vu.lt/lt/naujienos/ivykiu-kalendorius

Contents

Introduction 6
Relevance 7
The scientific tasks of this work 8
Novelty and importance 9
Statements to be defended 9
List of the author‘s publications related to thesis 10
Summary of doctoral thesis 10
Chapter 1. Literature survey 11
Chapter 2. Experimental techniques 11
Chapter 3. Self-start mode-locking of fiber lasers using semiconductor saturable absorber mirrors (SESAMs) 15
Chapter 4. The reliability of SESAM structures utilized in a fiber laser resonator 18
Chapter 5. The strategy to fabricate a reliable SESAM structure 23
Chapter 6. Single-wall carbon nanotubes for mode-locking of fiber laser 28
Chapter 7. The nonlinear optical properties of PbSe quantum dot and silver nanoprism saturable absorbers 32
Conclusions 34
References 36
Santrauka 39

Introduction

Here we introduce 2D, 1D and 0D nanomaterial saturable absorbers for self start mode-locking of fiber lasers. The locking of longitudinal modes in a resonator is the only way to produce ultra-short (<10 ps) pulses. By utilizing this technique for the fiber lasers and choosing a particular cavity configuration it is possible to tune pulse duration from many picoseconds down to several hundreds of femtoseconds. These ultra-short pulses are particularly important for femtochemistry [1], spectroscopy [2], two-photon microscopy and optical metrology [3]. However, it is extremely important to use the correct saturable absorber for different cavity configuration and only low-dimensional materials have the appropriate characteristics to self-start and hold stable long-term operation.

Semiconductor saturable absorber mirrors (SESAMs) are well known 2D nanomaterial based structures suitable for mode-locking of both the solid state and of the fiber lasers. However, the reliability of these devices depends on growth technology, materials and cavity design. For fiber lasers, SESAMs must possess higher nonlinearity than for solid state lasers. For this reason it is necessary to increase the number of active quantum well layers and use a higher field enhancement factor for the device. Both cases influence the damage thresholds of the SESAM. Therefore, we performed long-term (>5000 h) optical degradation tests of the high modulation depth saturable absorber. Also, we present results of experiments with the reliability of saturable absorbers utilized in different fiber laser configurations. Along with the results, we introduce a growth methodology to fabricate the low saturation fluence and high modulation depth SESAM, which is resistant to intense optical radiation. Also, we investigate the influence of different kinds of defects on the quantum well region.

SESAM reflects the great potential of low-dimensional structures to mode-lock ultra-short pulse fiber lasers. In order to compare the nonlinear optical properties of 2D, 1D and 0D nanomaterials, we also investigated single-wall carbon nanotube (1D) and PbSe quantum dot (0D) saturable absorbers. Unlike the SESAM, many low dimensional structures exhibit naturally fast recovery of optically excited carriers. Also, the saturation fluence of the device decreases with reducing the dimensionality of absorber material.

Another advantage of 1D and 0D semiconducting nanoparticles is the possibility to disperse them in a liquid environment. This feature enables us to fabricate a fiber integrated saturable absorber. As a consequence, the robust monolithic structure of an all-fiber laser with potentially trouble-free, long-term performance provides us with the opportunity to use them for medical or industrial applications [4]. However, the nonlinearity strongly depends on the size of the nanoparticle and laser wavelength. Therefore, it is necessary to choose a nanomaterial with the first excitonic state at the operating wavelength of a fiber laser.

Relevance

Currently, all commercial ultrafast lasers are mode-locked with a passive saturable absorber. Fiber lasers are an appropriate source of high power ultra-short pulses. Their single-mode maintenance-free operation, long-term thermal stability, low cost and compact size are very suitable for medical and industrial applications. Therefore, a reliable saturable absorber is necessary for a permanent trouble-free operation. Although SESAMs have been used for more than 25 years, there seems to be almost no scientific activity in researching for long lifetime SESAM architectures suitable for fiber lasers. Therefore, this work has been appointed to investigate the long-term performance of the saturable absorber in a fiber laser and the optical damage to the quantum well structure; also, to find the protocol to design a reliable SESAM. In order to design and manufacture the SESAMs with required nonlinear properties, we developed comprehensive characterization techniques for experimental evaluation of the grown structures. With this technique it was also possible to investigate different types of saturable absorbers and evaluate their suitability to mode-lock the fiber laser. For this type of lasers, fiber integrated devices are the most appropriate choice. Unlike the bulk quantum well structures, single-wall carbon nanotubes could be dispersed in a liquid and set near the core of an optical fiber. The new type of saturable absorber has great potential to increase the reliability and lifetime of a fiber laser. Furthermore, by controlling the type and diameter of single-wall carbon nanotubes, it is

possible to tune the nonlinear optical properties in a broad spectral region. However, low saturation fluence and high modulation depth of the saturable absorber must be maintained.

Our results were useful in developing commercial ultrafast fiber lasers and finding the protocol to increase the lifetime of a SESAM device.

The scientific tasks of this work

The main aim of this work was to adjust the nonlinear optical properties of the saturable absorber for proper operation of an ultrafast fiber laser. Also, to find the protocol to increase the lifetime of the device and maintain a reliable self-starting mode-locking operation.

To achieve these aims, the following tasks were performed:

1. Developing comprehensive saturable absorber characterization techniques for experimental evaluation of the grown and fabricated structures;
2. Comparing saturable absorbers with different nonlinear optical properties to define the best set of parameters for self-start mode-lock operation of a fiber laser;
3. Investigating the influence of the ultrafast laser radiation parameters on the lifetime of a saturable absorber and finding the protocol to reduce the risk of optical damage;
4. Determining the most reliable configuration of an ultrafast fiber laser.
5. Fabricating low saturation fluence and high modulation depth SESAM for fiber laser mode-locking at ~1 μm;
6. Finding and investigating alternative low dimensional structures to evaluate their suitability to mode-lock the fiber laser.

Novelty and importance

To our knowledge, the long-term (>5000 h) systematic study about gradual degradation of SESAM was performed for the first time. The necessity of slow degradation tests close to the operating conditions of SESAM was demonstrated from these results. The dependence of a SESAM lifetime on a fiber laser configuration was also shown.

The influence of the first excitonic state on nonlinear optical properties of the quantum well structure was demonstrated and an in-depth investigation was performed on the modification of its excited state lifetime with heavy and light ions. The importance of defect types on a saturable absorber's nonlinear parameters and reliability was also revealed.

The necessity to use the first excitonic state of a single-wall carbon nanotube instead of the second for fiber laser mode-locking was demonstrated. The increase of saturation fluence by two orders of magnitude for the second excitonic state was clearly shown. Also, the new type of fiber integrated saturable absorber was introduced and the ability to mode-lock the fiber laser was displayed.

We have clearly demonstrated the possibility to reduce the saturation fluence of a saturable absorber, starting from 2D structures (SESAMs) and ending with 0D (quantum dots) materials. Also, we presented the dependence of other nonlinear parameters on fabrication technology and material properties.

Statements to be defended

1. Reliable self-start mode-locking of a fiber laser can be ensured when the saturation energy of an absorber is one order of magnitude lower than the circulating pulse energy in a resonator, while the minimum modulation depth must be higher than 4 %.
2. Depending on a pulse fluence, the optical properties of SESAM can be modified in two different ways – at high fluencies (S>73), critical optical damage occurs in less than 24 h and decreases the linear reflectivity, whereas at lower fluencies (S<35), slow (>1000 h) degradation of nonlinear optical parameters is observed.

3. It was determined that the highest modulation depth and lowest saturation fluence of SESAM is at the first excitonic absorption state wavelength of quantum wells, the spectral position of which could be controlled during the growth process of the semiconductor structure.
4. By choosing the right diameter of single-wall carbon nanotubes, it is possible to fabricate a saturable absorber with the first excitonic absorption state at the laser wavelength.
5. By measuring the nonlinear absorption of single-wall carbon nanotube saturable absorber, it is possible to distinguish the different chirality of familiar diameter nanoparticles.

List of the author‘s publications related to thesis

1. **K. Viskontas** and N. Rusteika, *All-fiber wavelength-tunable picosecond nonlinear reflectivity measurement setup for characterization of semiconductor saturable absorber mirrors,* Opt. Fiber Technol., 31 (2016), 74-82 (2016).
2. **K.Viskontas**, K.Regelskis and N.Rusteika, *Slow and fast optical degradation of the SESAM for fiber laser mode-locking at 1 μm* , Lith. J. Phys., 54 (3), 127-135 (2014).
3. J. Zeludevicius, K. Regelskis, **K. Viskontas**, and G. Raciukaitis, *Yb-doped fiber ultrashort pulse generator based on self-phase modulation and alternating spectral filtering*, Optics Letters, Vol 40, isue 22, pp.5255-5258 (2015).
4. J. Zeludevicius, R. Danilevicius, **K. Viskontas**, N. Rusteika, and K. Regelskis, *Femtosecond fiber CPA system based on picosecond master oscillator and power amplifier with CCC fiber,* Optics Express, Vol. **21**, Issue 5, pp. 5338-5345 (2013).

Summary of doctoral thesis

The doctoral thesis consists of 7 chapters. Except for the first chapter, other six contain experimental results, including all-fiber characterization techniques for experimental evaluation of the fabricated saturable absorber structures. The detailed overview of separate chapters is given below.

Chapter 1. Literature survey

In this chapter, the basics of the mode locking theory with fast and slow saturable absorber are reviewed. Also, the differences between ultra-short pulse generation in solid state and fiber lasers are introduced. Although there are similarities between these types of laser, requirements for nonlinear parameters of saturable absorber strongly depend on the dispersion in a fiber resonator. Only low-dimensional semiconductor materials satisfy these conditions and, therefore, their linear and nonlinear optical properties are presented. SESAMs have quantum well absorber layers which are a 2D structure. To compare it with other lower dimension nanomaterials, single-wall carbon nanotubes (1D) and PbSe quantum dots (0D) are reviewed.

Chapter 2. Experimental techniques

A particular set of absorber nonlinear parameters is required to achieve self-starting mode-locking and avoid undesirable q-switch mode-locking for the ultra-short pulse laser [5]. To investigate the nonlinear properties of saturable absorbers, the methodology and experimental setups to measure the nonlinear reflectivity and pump-probe are introduced in this chapter. Also, the basic types of absorber integration into an optical fiber are presented. We also introduce the fitting function to determine all nonlinear parameters of a saturable absorber.

For the experiments, ultrashort optical pulses were generated from a SESAM mode-locked picosecond fiber oscillator with a tunable center wavelength. The resonator consisted of chirped fiber Bragg grating (CFBG), an ytterbium-doped polarization maintaining (PM) single-mode fiber (YDFO), a fiber coupled tunable wavelength filter (TWF), a micro-optical fiber pigtailed beam splitter (PBSO) and a SESAM with a high nonlinear modulation depth (ΔR>25 %) within a broad spectral range (Fig. 1a). The oscillator was pumped by a laser diode (LD) with the center wavelength of a 976 nm. Isolator (ISO) and a wavelength division multiplexer/optical isolator hybrid (WIDM) were used to couple the oscillator output with the preamplifier stage. In the operating wavelength range 1020-1074 nm (Fig. 1b), it produced ~6-9 ps pulses with the maximal energy of 1.5 nJ after the preamplifier. At

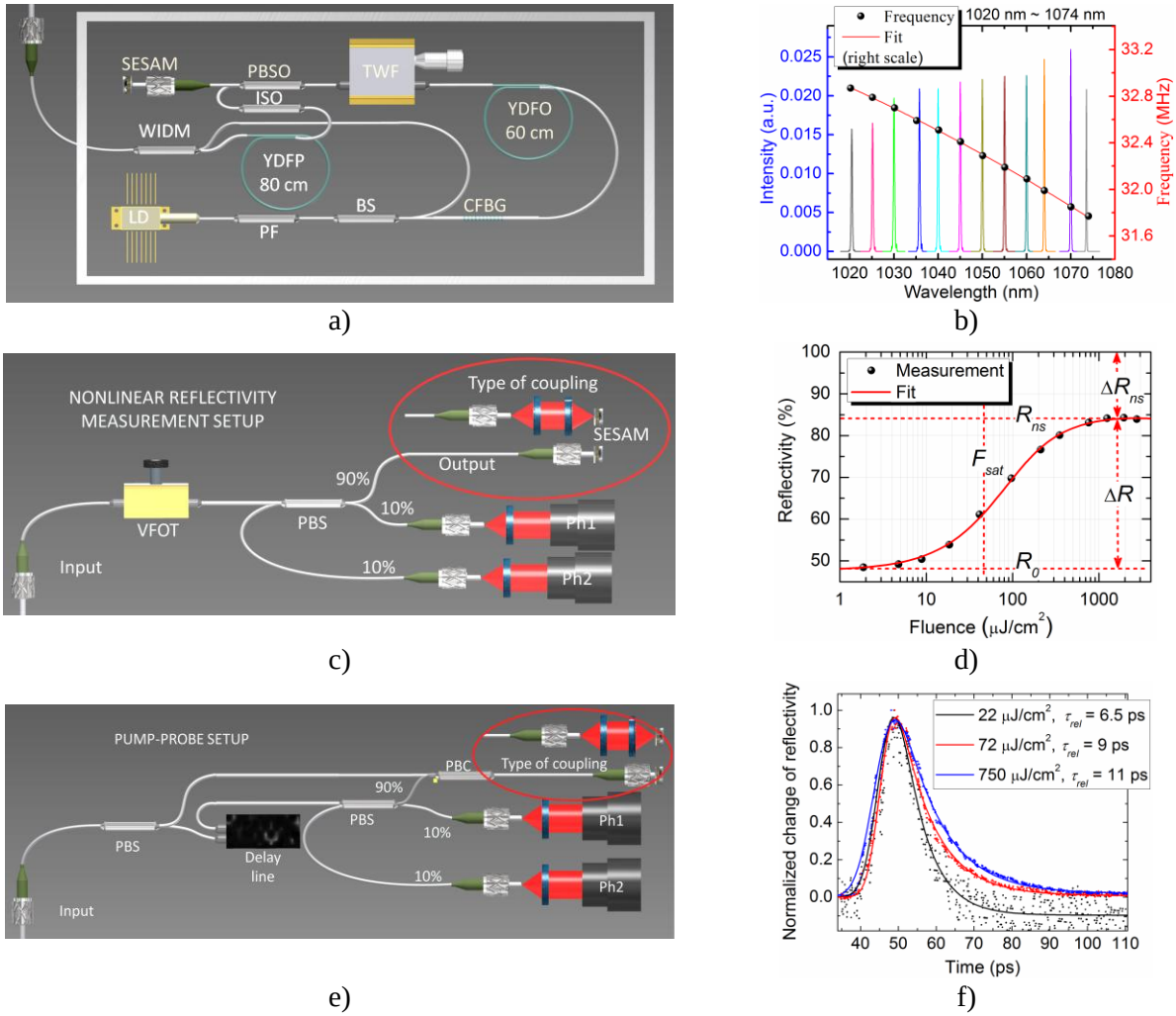

Fig. 1. All-fiber nonlinear reflectivity and excited carrier relaxation time measurement setups for characterization of saturable absorber mirrors: a) the tunable oscillator with a preamplifier used for the measurements; b) the spectra of the continuously tunable mode-locked fiber oscillator (color solid lines, left scale) and the frequency of an oscillator at different wavelengths (black data points, right scale); c) the nonlinear reflectivity measurement system; d) nonlinear reflectivity of a typical SESAM device; e) the pump-probe measurement system: PBC – fiber micro-optic polarization beam combiner for combining pump and probe optical pulses which are separated in time using a variable delay line; f) typical SESAM pump-probe measurement at different pulse fluences.

this pulse energy, achievable energy fluence was ~4000 μJ/cm^2 assuming a 6.6 μm beam diameter (equal to the mode field diameter of a single mode optical fiber) on the sample.

There are two basic techniques to determine the nonlinear parameters of a saturable absorber – the nonlinear reflectivity measurement and the pump-probe experiment. The first one measures the absorber reflectivity as a function of an incident optical pulse energy fluence. The experimental setup with main optical elements is shown in Fig. 1c. In order to change the optical power (fluence) on the sample, the variable fiber optical attenuator

(VFOT) was connected to the laser output. A micro-optical fiber pigtailed beam splitter with a 90/10 splitting ratio provided three outputs – to the sample (90% output), to the reference detector (10% Ph1) and to the reflection channel detector (10% Ph2). To detect the signals at the reflection and reference channels two photodiode power sensors (Thorlabs S130C) with a dual-channel power meter console (Thorlabs PM320E) were used. In order to determine the absolute value of sample reflectivity, a fiber pigtailed mirror with the insertion loss of 0.8 dB was used as a reference to calibrate the system and eliminate the nonlinearity of photodiodes. Over the whole spectral range (1020-1074 nm), less than 1% of absolute nonlinear reflectivity accuracy was demonstrated. The repeatability of a reflectivity measurement was better than 0.06%. The achieved fluence ranged from 100 nJ/cm^2 to 2 mJ/cm^2 with a corresponding intensity from 10 kW/cm^2 to 300 MW/cm^2. Using the setup, all static non-linear response parameters of a saturable absorber can be found by fitting the experimental data to the equation (1) [6]

$$R(F_p) = 1 - \Delta R_{ns} - \Delta R \frac{1 - e^{(-F_p / F_{sat})}}{F_p / F_{sat}} - F_p / F_2. \qquad (1)$$

Here F_{sat} is the saturation fluence, ΔR - modulation depth, R_0 - low intensity reflectivity, R_{sat} - saturated reflectivity and ΔR_{ns} - nonsaturable losses (Fig 1d). The main advantage of an all-fiber configuration is the simplicity of measuring the fiber-integrated or fiber-pigtailed saturable absorbers in ultrafast regime.

The excited carrier relaxation dynamics of saturable absorbers are also very important for the soliton pulse stabilization process [5]. The approximate limit of maximum permissible value of relaxation time for a saturable absorber is $\tau_A < 28\tau_p$ [7], where τ_p is the duration of a soliton pulse. Therefore, the measurement of pulse relaxation time is vital to evaluate the suitability of a saturable absorber for mode-locking of fiber lasers. The experimental setup is shown in Fig. 1e. The setup was connected to another mode-locked fiber laser which provided ~2 ps pulses at fixed 1064 nm wavelength and ~700 pJ pulse energy. The input pulses were separated into pump and probe with a fiber beam splitter (PBS). 90% of pulses were provided to the sample (pumping) and 10% to the motorized

fiber-coupled delay line (for probing) which allowed to vary the time interval between them with the resolution of ~7 fs. After the delay line, the probe pulses were split in another beam splitter which provided three outputs - to the sample (90%), to the reference detector (10% Ph1) and to the reflection channel detector (10% Ph2). These detectors provided the ratio between the applied and the reflected probe signal. The main component to combine the pump and probe pulses on the sample was the micro-optic polarization beam combiner which also separated them after the reflection. The example of a pump-probe measurement of a SESAM at different pulse fluences is shown in Fig. 1f.

Another important task was to couple the saturable absorber with the optical fiber. It is desirable to control the spot size to increase the energy fluence [49] or to reduce the thermal load on absorber material [8]. The spot size on a fiber butt-coupled sample is equal to the mode field diameter of a fixed single mode fiber. Two different methods are used in order to change it. The conventional way is to use free-space or micro-optic lenses. But the concept of a monolithic fiber laser with a robust no-alignment operation is compromised; therefore, we introduce an all-fiber solution of optical probing, using a gradient index fiber (GRIN). Image of GRIN fiber GIF625 end-caps which was spliced to the large core diameter (~100 µm) fiber AFS105 is shown in Fig. 2a. The piece of AFS105 fiber was used to extend the initial beam radius before entering the GRIN fiber (Fig. 2b). The length of GRIN fiber end-

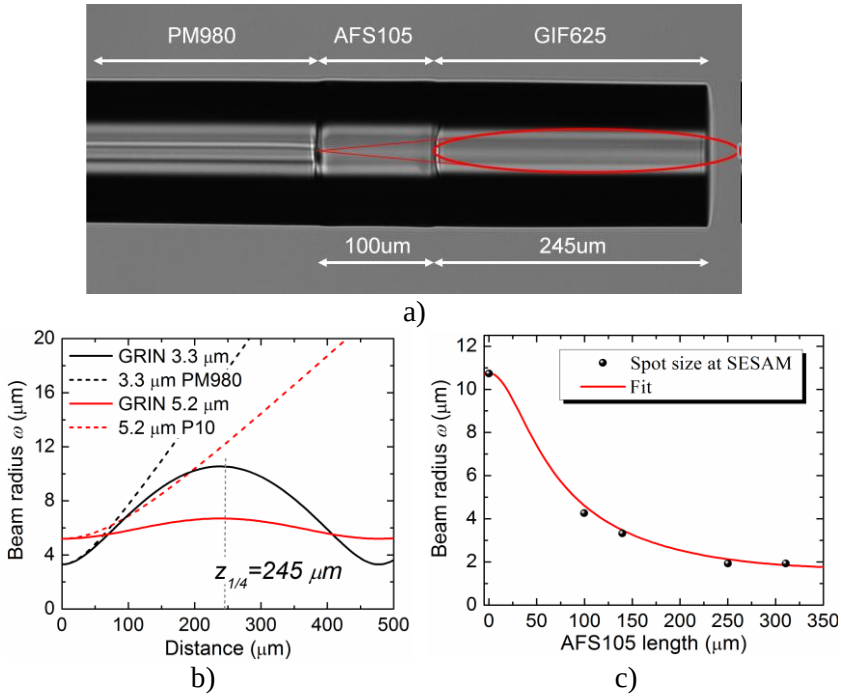

Fig. 2. Spot size variation using a gradient index fiber. a) Image of GRIN fiber end-caps spliced to the large core diameter (~100 µm) AFS105 fiber which is used to extend the output beam radius. b) The comparison of beam radius evolution in a GRIN fiber (solid lines) and AFS105 fiber (dashed lines). c) Variation of spot size on a SESAM changing the AFS105 fiber length between a single mode fiber (PM980) and GRIN fiber (GIF625) end-caps.

caps was a critical parameter – the end-caps had to be cut exactly at ¼ pitch length [9]. This allowed us to use the fiber as a thick lens and change the spot size on an absorber (Fig. 2c). Therefore, it was possible to change the saturation fluence of a SESAM by varying the length of the AFS105 fiber.

Chapter 3. Self-start mode-locking of fiber lasers using semiconductor saturable absorber mirrors (SESAMs)

In this chapter, the influence of nonlinear saturable absorber parameters on fiber laser mode-locking was studied in detail. In order to mode-lock the fiber laser, it is necessary to use a SESAM with higher modulation depth than in solid state lasers [10]. Loss modulation must be large enough to initiate self-start mode-locking of a fiber laser, but should not exceed the limit value in order to prevent Q-switching instabilities. The condition for self start mode-locking of fiber laser with a SESAM is [5]

$$\frac{-\ln(1-R_{ns}-\Delta R)}{E_{sat}/\tau_{rel}} > \frac{\gamma_{NL} L_{rt}}{|D_2|\Delta\omega_b^2}, \qquad (2)$$

where R_{ns} and ΔR are nonsaturable reflectivity losses and modulation depth of a SESAM. The other parameters on the left side define the saturation power of the saturable absorber, which is the ratio between the saturation energy E_{sat} and relaxation time τ_{rel}. The right side of the equation (2) is related to the fiber laser resonator. Here D_2 is the group delay dispersion (GDD), L_{rt} – the round-trip length and $\Delta\omega_b$ – the bandwidth (FWHM) of spectral filtering. γ_{NL} is the nonlinear parameter of SPM [11]. Thus, the self-start mode-locking of a fiber laser is easier to achieve with higher dispersion values of the resonator.

The other condition for reliable mode-locking of a fiber laser is to avoid Q-switch instabilities. This condition is written by [5]

$$\frac{q_0}{P_A} P_{ave} < \frac{T_{rt}}{\tau_g}\left(1+\frac{P_{ave}}{P_s}\right). \qquad (3)$$

Here $q_0 = -\ln(1-R_{ns}-\Delta R)$ and P_A is the saturation power of a saturable absorber. P_{ave} is the average power, P_s and τ_g is the saturation power and upper laser layer lifetime of gain medium [12], T_{rt} is the round trip time. According to this condition, the modulation depth of saturable absorber must be as low as possible, but this contradicts to the condition (2).

Consequently, the modulation depth must be high enough to initiate mode-locking, but not too high to avoid Q-switch instabilities. This is particularly important for low dispersion values of a fiber resonator where the modulation depth must be very high to stabilize the laser.

To find and optimize the nonlinear parameters of a saturable absorber for reliable self-start mode-locking of fiber laser, experiments with different types of SESAMs were performed. The principal optical scheme of fiber laser which was pumped by 976 nm laser diode (LD) is shown in Fig. 3a. It consisted of ytterbium-doped fiber (YDF), fiber micro-optic beam splitter (PD) and chirped fiber Bragg grating (CFBG) on one side and the SESAM on the other side of resonator. In the experiments, the GDD value of CFBG was ~14 ps/nm, which is opposite-sign and much higher than the total dispersion of optical fiber in the resonator (-0.1 ps/nm). Hence, CFBG defined the total dispersion of fiber laser. The main laser parameters were: pulse duration τ_p~5 ps, pulse repetition rate ν = 38 MHz, dispersion D_{CFBG} = 14 ps/nm, spot diameter on a SESAM d~6.6 μm, pulse energy E_p~400 pJ. The typical structure of a high modulation depth SESAM is shown in Fig. 3b. To investigate the mode-locking of fiber laser, several different types of SESAMs were ordered from *Batop* of which the nonlinear optical parameters are listed in Table 1.

Table 1. The nonlinear optical parameters of SESAMs used in the experiments.

SESAM type	ΔR	F_{sat}	τ	Structure
I	36	47	15	Anti-resonant
II	26.6	37	7	Anti-resonant
III	12.5	44	5	Anti-resonant
IV	7.4	6	16	resonant
V	7.1	39	5	Anti-resonant
VI	5	5	10	resonant
VII	5	33.5	5	Anti-resonant
VIII	3	43	1	Anti-resonant

All SESAM were tested in the resonator of the fiber laser. The self-start mode-locking was achieved with all SESAM, except for the VIIth, with the lowest modulation depth (ΔR = 3%). This exception was in a good agreement with condition (2), which is graphically shown in Fig. 3c. Here, solid curves were drawn using the left side in eq. (2) by varying the modulation depth and using two different values of saturation fluence – 40 μJ/cm^2 (red) and 6 μJ/cm^2 (blue) at fixed relaxation time (7 ps). The dashed line represents the right hand

side of the equation and was drawn using the described parameters of the fiber laser. Upon inserting the modulation depth values of real SESAMs (data points), it becomes clear that 3% was below the minimum value to initiate self-start mode-locking of the laser. Also, laser with a SESAM VII (see Table 1) was not stable at the mode-locking threshold. This was not the case for SESAM VI with the same modulation depth (ΔR = 5%), but more than six times of lower saturation fluence.

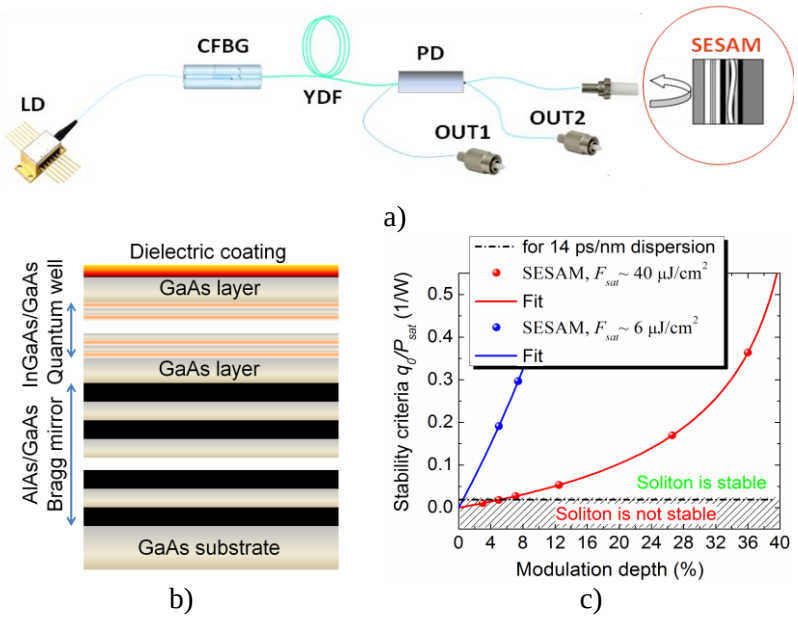

Fig. 3. a) A principal optical scheme of picosecond fiber oscillator used in the study. b) Typical structure of high modulation depth InGaAs/GaAs SESAM. InGaAs QWs consists of ~10-20 single well layers (thickness ~10 nm), Brag reflector composed of AlAs/GaAs multilayer containing 15-25 periods. c) Soliton pulse stability criteria of an oscillator using SESAMs with different nonlinear reflectivity parameters. At the fixed resonator dispersion value (~14 ps/nm) to stabilize the soliton pulse the minimum requirement of nonlinear modulation depth is lower for SESAMs with low saturation fluence (blue line).

There is a stability interval for soliton pulses, also called the operating window (DL), which defines the reliable performance of a fiber laser. According to the maximum allowed nonlinear phase shift in a fiber laser [4] and soliton stability condition [5], one could write

$$DL = \sqrt{\frac{D_2}{D_g}\frac{\Delta R}{P_A}}. \qquad (4)$$

Accordingly, the stable operating window depends on both – the saturable absorber and the dispersion of a fiber resonator. The validity of (4) was experimentally verified and is shown in Fig. 4a, where data points from measured operating windows of the fiber lasers are plotted together with the curves and calculated using this simple formula. The red solid line was calculated using F_{sat} = 40 μJ/cm^2 and τ_r = 7 ps values, which are close to the values used in the experiment. Two data points in Fig. 4a were outside of the solid line, but in changing the saturation fluence in (4) to the real values of SESAM IV (dashed line) and VI

(dotted line), the calculated results were in good agreement with the measured ones. For a fixed dispersion value of fiber resonator, the higher modulation depth is desirable to have a reliable operating window.

To investigate further, the dispersion of fiber resonator was varied from 14 ps to 1.6 ps by changing the chirped fiber Bragg grating (Fig. 4b). Then the experiment values of the operating window were compared to the calculated ones using eq. (4). Only the highest modulation depth of SESAM I was used in these experiments. The experimental values (data points) were within the calculated curve (solid curve). Therefore, even with extremely high modulation depth (36 %), the operating window is relatively narrow for the lowest dispersion values.

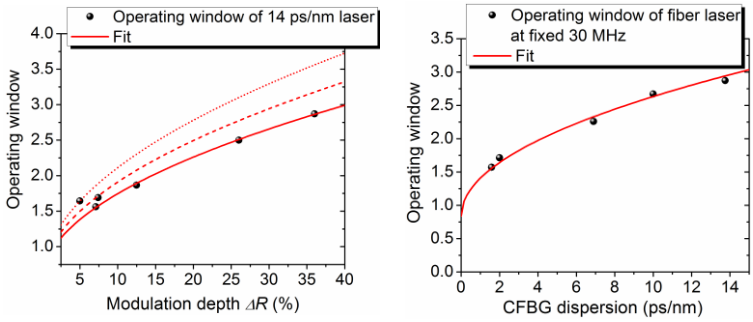

a) b)

Fig. 4. Operating window of soliton lasers. a) The operating window between single pulse and double pulse regimes of oscillator depends on the modulation depth of a SESAM if all other nonlinear parameters are fixed. b) Operating window also depends on dispersion value of laser resonator.

Chapter 4. The reliability of SESAM structures utilized in a fiber laser resonator

In this section, a detailed study of degradation of quantum well (QW) based semiconductor saturable absorber mirror irradiated with picosecond pulses from a fiber laser at ~1 μm wavelength was introduced. For operational wavelength of the Yb-doped fiber lasers (typically 1000 – 1100 nm), SESAM based on $In_xGa_{1-x}As/GaAs$ super-lattice saturable absorber and AlAs/GaAs Bragg mirror is a common choice. The higher modulation depth which is necessary for mode-locking of fiber lasers is usually achieved by increasing the number of InGaAs quantum wells. However, this leads to excessive mechanical strain within the device as the absorber layers are often not exactly lattice-matched to the Bragg mirror structure [13]; in turn, they can make SESAM more susceptible to optical damage or lead to faster optical degradation. Recently, instant damage studies were performed for SESAMs with a small nonlinear modulation depth, predicting

the lifetime of a device [14]. We set to investigate the slow and fast optical degradation and reliability of high modulation depth SESAMs which are suitable for the mode-locking of fiber lasers at 1 μm. The aim was to find a protocol for the accelerated lifetime tests of the device.

Table 2. The nonlinear parameters of SESAMs used in the optical degradation study.

SESAM type	F_{sat}, μJ/cm^2	ΔR, %	R_{ns}, %	τ_{rel}, ps
I	35	27	15	1
II	47	37	15	15
III	20	22	13	7

In this study, different commercially available SESAMs produced by *BATOP* were investigated (see Table 2). For degradation studies, the reflectivity of SESAMs was monitored continuously by measuring reference and reflected power from the SESAM which was directly used in a fiber laser resonator – the source of ultra-short pulses. The principal scheme of the laser was similar to that shown in Fig. 3a. It was assumed that the degradation will lead to the reduction of the reflectivity. The time dependent degradation of normalized reflectivity was fitted using a single exponential function with the offset:

$$R_N(t) = 1 - dR \cdot e^{-\frac{t}{\tau_d}}, \tag{5}$$

where dR is the total drop of reflectivity (at $t >> \tau_d$), τ_d is the decay time, during which 63% (1-1/e) of the total drop of reflectivity occurred. The SESAM was butt-coupled to the FC/PC connector of an optical fiber (Fig. 5a). The results of the slow optical degradation of the type I (τ_{relax} = 1 ps) and type II (τ_{relax} = 15 ps) SESAMs are shown in Fig. 5 (here the saturation parameter is $S = F_p/F_{sat}$). The main finding was a tendency that the SESAMs with the slower (15 ps) carrier relaxation time (curve 2 and curve 3) showed considerably longer lifetime (~5000 h) in the mode-locked fiber laser compared to the SESAM with the faster carrier relaxation (1 ps, ~1000 h, curve 4). At the lower repetition rate and reduced thermal load the expected lifetime was forecasted to be well above 10000 h, but the laser stopped working at 9300 h. Also, we performed the non-linear reflectivity measurement of SESAMs before and after the degradation experiments. The results for the type II SESAM (S_2 = 25 and ν_2 = 46 MHz) are shown in Fig. 5c. The modulation depth ΔR of this particular SESAM decreased from 37% to 14% and saturation fluence F_{sat} increased from 45 μJ/cm^2 to

230 μJ/cm^2. The largest change was observed for the coefficient of the inverse saturable absorption (ISA) F_2 which decreased from 700 mJ/cm^2 to 38 mJ/cm^2. Therefore, this change was assigned to some defects created in the InGaAs quantum wells.

The accelerated damage test (Fig. 5d) with type III SESAM revealed that the mechanism of the degradation at the higher saturation levels (S = 73-118) was different than that of the slow degradation at the lower saturation (S = 25-34). After the reflectivity decayed by ~2% (lowest fluence) to ~10% (highest fluence), all samples experienced the catastrophic optical damage (COD) which was observed as a sudden drop of reflectivity by ~30% from the initial value. The non-linear reflectivity measurements before and after the COD (Fig. 5e) revealed that a relative modulation depth ($\Delta R/R_{ns}$) did not change significantly (decreased from 0.35 to 0.33), the saturation fluence slightly increased from 20 to 27 μJ/cm^2 and ISA coefficient reduced from ~200 mJ/cm^2 to ~70 mJ/cm^2.

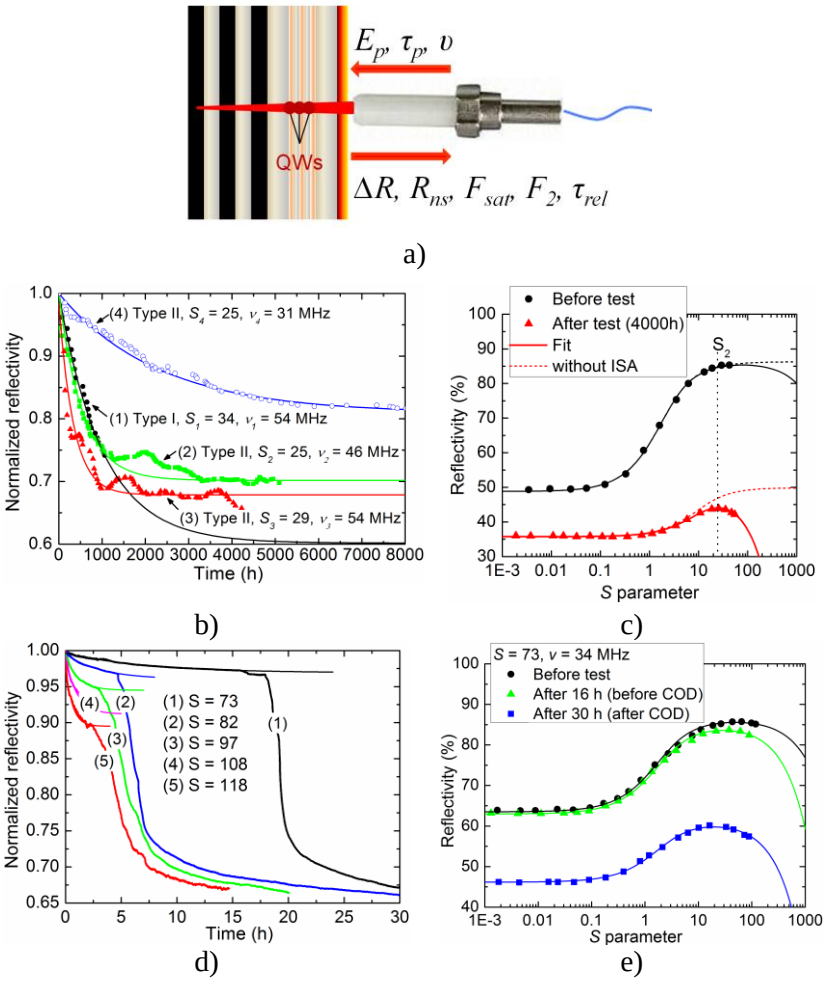

Fig. 5. Slow and fast optical degradation of the SESAM. a) By using butt-coupling of SESAM to the single mode fiber, it is possible to investigate the change of nonlinear reflectivity parameters over a long period of time within a single spot. b) Slow degradation of *in-situ* reflectivity of the type I and type II SESAMs. c) Results of the non-linear reflectivity measurement of the type II SESAM before (black circles) and after (red triangles) 4000 h of the optical degradation test at the saturation level S_2 = 25 and the repetition rate ν_2 = 46 MHz. d) Fast optical degradation of type III SESAM reflectivity (normalised) at different values of the saturation parameter. Results of the non-linear reflectivity measurement of the type III SESAM at the beginning of the fast degradation test (black circles), after 15 hours of exposure (green triangles), and after COD (blue squares) along with the fitting curves (solid lines).

However, the majority of the ISA change (from ~200 mJ/cm^2 to ~80 mJ/cm^2) occurred in the phase of the exponential decay before COD. Therefore, it was deduced that the mechanism of the critical optical damage at high fluencies is predetermined by the increase of two-photon absorption which most likely occurs after the optical damage of GaAs material outside the quantum well region.

The influence of a nonlinear process on the COD of a SESAM is evident from the investigation of a damage spot (Fig. 6a). As the intensity at the central part of the mode is e^2 times higher (source for two-photon absorption) than the intensity at the "edge" (distance from the center equal to the mode field radius); this is the reason for the very small size of the damaged spot compared to the mode field diameter of the optical fiber. In contrast, the thermal distribution is almost identical far away from the central part of the spot (Fig. 6b). This could be the case for slow degradation tests where the pulse peak intensity is moderate. Therefore, the possible thermally induced damage to the quantum well region includes a large area of an illuminated spot and the absorber nonlinear parameters degrade more than twice.

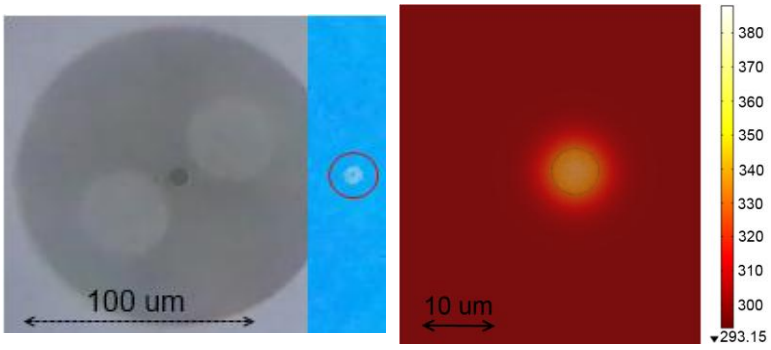

a) b)

Fig. 6. Degradation of SESAM parameters in ultra-fast fiber lasers. a) On the left: microscope image of a fiber end-face used to pigtail the SESAMs. On the right: microscope image with the same magnification of the affected area (encircled) of the type III SESAM after COD at the highest saturation level of S = 118. The darker spot ~2µm is clearly visible at the center of this area. b) Modeling of temperature distribution in a structure containing InGaAs quantum wells and GaAs substrate. The applied optical intensity was I = 50 kW/cm^2.

In order to confirm the degradation model, the high modulation depth type II SESAM was further investigated in nine different configurations of fiber laser resonators which are listed in Table 3, together with the nonlinear parameters of SESAM, measured after long-term degradation study. The main discovery was the linear increase in modification speed of saturation fluence when increasing the average intensity on a SESAM (Fig. 7a). Also, measuring the F_{sat} modification during the single shot, it was possible to determine the optical damage initiation threshold for the saturable absorber, which was ~200 µJ/cm^2 or S

= 4.4 (Fig. 7b). This saturation parameter is typical for solid state lasers, but for fiber lasers S is usually above 10. The type II SESAM, which was used in the resonator of lowest dispersion laser (with S = 9), had the best lifetime and was able to stabilize the soliton pulses even after 18 000 h of operation.

Table 3. The nonlinear parameters of type II SESAM after the long term degradation study.

Initial parameters of fiber laser					**SESAM parameters after the study**					
Laser		**Repet.**	**Pulse**	**Power**	R_{ns}	ΔR	F_{sat}	τ_r	**Op.time**	**Number of pulses**
No.		ν, **MHz**	τ_p, **ps**	P_0, **mW**	**%**	**%**	**μJ/cm^2**	**ps**	t, **h**	
14 ps/nm 1064 nm	1	20	5.2	6.5	46	17	182	4	9800	$7.0*10^{14}$
	2	31	5.7	13	37.5	15.5	150	5	6630	$7.4*10^{14}$
	3	40	6.5	14	53	14	300	3	6650	$9.6*10^{14}$
7 ps/nm 1064 nm	4	31	3.5	10	40	18	279	5	9312	$10.4*10^{14}$
	5	47	4.5	16	49	16	325	5	6072	$10.3*10^{14}$
	6	54	4.9	20	45.6	16.7	311	4	4440	$8.6*10^{14}$
2 ps/nm 1064 nm	7	40	2.1	5	21	35	82	5	10800	$15.5*10^{14}$
	8	50	2	10	52	17	160	5	5040	$9.1*10^{14}$
1.6 ps/nm	9	30	1.5	4.5	-	-	-	-	18000	$19.4*10^{14}$

The interplay between thermal and two-photon absorption effects in the SESAM was evident from the nonlinear reflectivity measurements of saturable absorbers which were used in two different lasers – No.2 and No.7 (Fig. 7c). Higher drop of linear reflectivity was observed for SESAM used in laser No.7, but the nonlinear modulation depth of the device degraded stronger in laser No.2. As the peak intensities of both lasers were comparable (~300 MW/cm^2), the main reason of different ΔR degradation nature had to be related to the average power. The saturation fluence of SESAM used in laser No.2 also degraded faster. Hence, the best lifetime of a SESAM could be achieved in a fiber laser the pulse energy and repetition rate of which are as low as possible.

The pump-probe measurements of type II SESAMs after long-term degradation tests revealed the reduction of relaxation time (Fig. 7d). The main mechanism of a fast carrier relaxation in SESAMs is a high number of defects in a quantum well region. Therefore, the decrease of SESAM relaxation time may be related to the generation of new defects after the long term irradiation of saturable absorber layers. The highest change of relaxation time for SESAMs was the one during which nonlinear parameters degraded fastest (used in highest dispersion lasers).

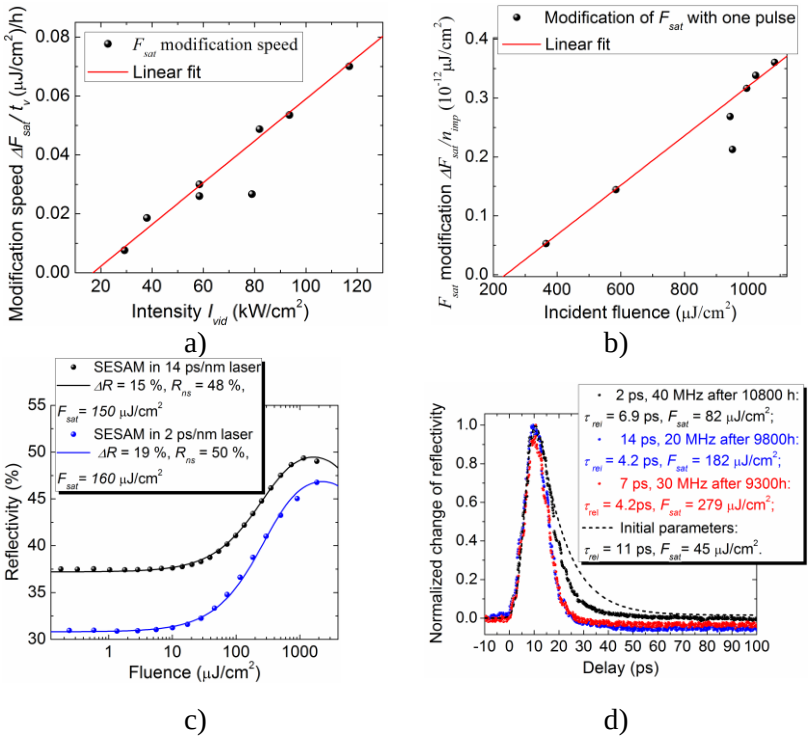

Fig. 7. a) Modification speed of saturation fluence F_{sat} using different average intensity on the SESAM surface (data points). b) F_{sat} modification within a single pulse shot which almost linearly depends on the incident pulse fluence. c) Results of the non-linear reflectivity measurement of the type II SESAMs utilized in fiber laser resonators with two different cavity dispersions (14 ps/nm and 2 ps/nm) after ~5000 h of the slow optical degradation test. d) Change of excited carrier relaxation time of the type II SESAMs used for long term degradation study in the fiber resonators with three different dispersion values: 14 ps/nm, 7 ps/nm and 2 ps/nm.

Chapter 5. The strategy to fabricate a reliable SESAM structure

Here, the special high quality SESAM structure was grown to reduce the growth defects in the quantum well absorber layers. To achieve a sufficiently low saturation fluence of the device which is necessary for reliable self-starting performance of a fiber laser, the first exciton absorption peak was adjusted to be near the operating laser wavelength. In order to reduce the carrier relaxation time of a saturable absorber, the grown SESAM structure was implanted with two types of ions – heavy (Arsenic) and light (Hydrogen). Then, the best SESAM was tested in a fiber laser resonator to verify the mode-locking performance.

SESAM was grown at high temperature (~500 ^{0}C) in order to have high quality

semiconductor layers [15]. The structure consisted of three InGaAs quantum wells, GaAs spacer and GaAs/AlAs Bragg mirror layers (Fig. 8a). The clear excitonic feature is visible in the measured quantum well absorption spectra (Fig. 8b). The nonlinear reflectivity

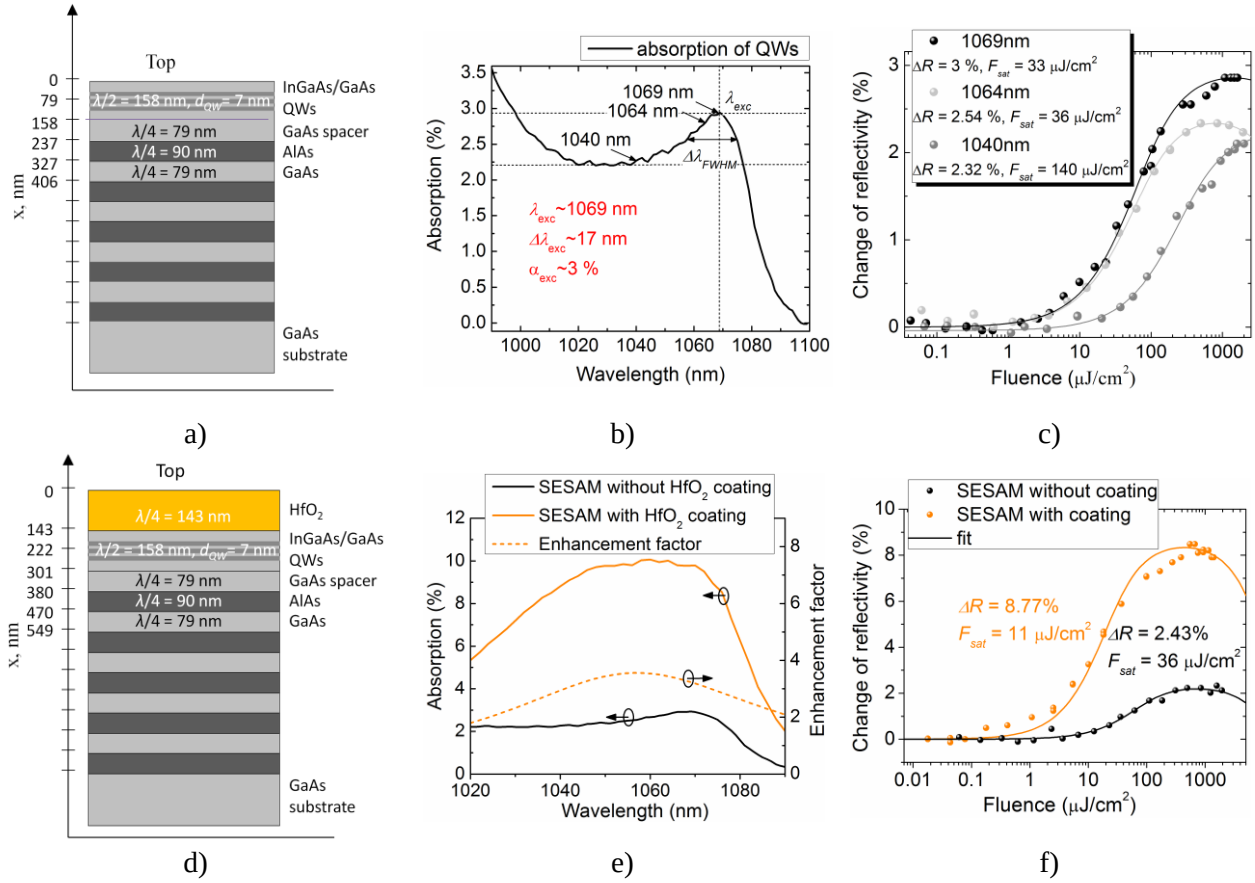

Fig. 8. The linear and nonlinear optical properties of grown SESAMs. a) Anti-resonant SESAM structure; b) the absorption spectra of quantum wells; c) change of nonlinear reflectivity of anti-resonant SESAM at different wavelengths – 1069 nm, 1064 nm and 1040 nm. d) Resonant SESAM structure; e) absorption spectra of quantum wells in a resonant SESAM structure. The enhancement factor define the ratio between resonant and anti-resonant optical field intensity inside the absorber layers; f) change of nonlinear reflectivity of anti-resonant and resonant SESAMs measured at 1064 nm wavelength.

measurement of the SESAM around the quantum well absorption maximum revealed the low saturation fluence (<40 μJ/cm^2) at 1069 nm and 1064 nm wavelengths, but high saturation fluence at 1040 nm wavelength (Fig. 8c). The low saturation fluence was attributed to the low dimensionality of quantum wells. To increase the modulation depth, the additional HfO_2 layer was coated on the anti-resonant SESAM top layer to have the resonant structure (Fig. 8d). The enhancement of the linear absorption of a coated SESAM structure is shown in Fig. 8e. The nonlinear reflectivity measurement of the SESAM at 1064 nm revealed the change of both parameters – modulation depth and saturation fluence (Fig.

8f).

In order to reduce the initial relaxation time of the grown SESAM, the structure was irradiated with two types of ions – heavy (As) and light (H). The irradiation was done using a *Tandetron* 4110A ion accelerator. Results of nonlinear reflectivity and pump-probe measurements are shown in Fig. 9. Arsenic ions were implanted for both – anti-resonant and

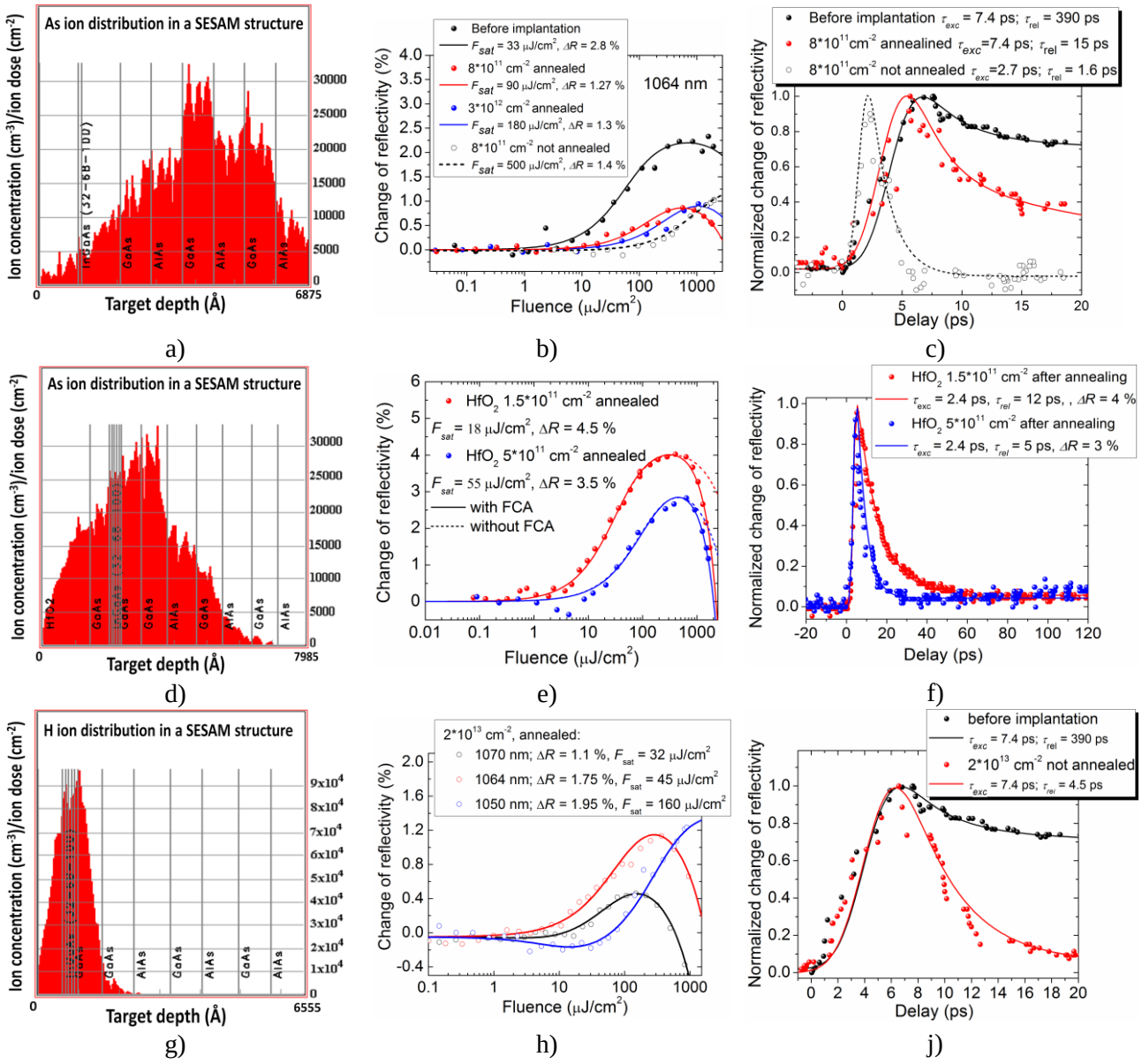

Fig. 9. a) As ion implantation into the anti-resonant SESAM structure with two different doses: $8*10^{11}$ cm^{-2} and $3*10^{12}$ cm^{-2}: a) modeling experiment; b) the change of nonlinear reflectivity; c) the pump-probe measurements at 1064 nm wavelength.. As ion implantation into the resonant SESAM structure with two different doses: $1.5*10^{11}$ cm^{-2} and $5*10^{12}$ cm^{-2}: d) modeling experiment; e) the change of nonlinear reflectivity; f) the pump-probe measurements at 1064 nm wavelength. H ion implantation into the anti-resonant SESAM structure with $2*10^{13}$ cm^{-2} dose: g) modeling experiment; h) the change of nonlinear reflectivity; j) the pump-probe measurements at 1064 nm wavelength.

resonant SESAM structures. Modelling using TRIM ("Transport of Ions in Matter") program showed the deeper penetration of these ions into anti-resonant SESAM structure without a HfO_2 coating (Fig. 9a and d). The nonlinear reflectivity measurements indicated significant reduction of modulation depth and increase in saturation fluence even after long annealing at high temperature (20 min. 600 ^{0}C) (see Fig. 9b and e). However, the change of nonlinear parameters was higher for higher implanted ion doses. Although the relaxation time decreased from ~390 ps to less than 15 ps for both types of SESAM structures (see Fig. 9c and f), the carrier excitation time was different. After annealing, the carrier excitation time for the anti-resonant SESAM structure reached the initial value of ~7.4 ps, while for the resonant SESAM the carrier excitation time remained very fast at ~2.4 ps. This was attributed to the different kind of high energy defects outside the quantum well structure. The implantation of H ion into the SESAM structure (Fig. 9g) also resulted in the degradation of nonlinear parameters (Fig. 9h), but required relatively modest annealing (5 min., 300 ^{0}C). To reduce the SESAM relaxation time to less than 15 ps it was necessary to implant two orders of magnitude higher H ion dose than As ion dose. The carrier excitation time remained close to the initial value (~7.4 ps) even before the annealing.

The measurements of linear absorption spectra after the implantation of anti-resonant SESAMs with two different types of ions (Fig. 10a) showed clear broadening of the excitonic feature and a shift to shorter wavelengths for the As ion implanted sample (black curve). This was not the case for the H ion implanted sample (red curve). However, the small shift of excitonic feature wavelength was also observed. The change of SESAM

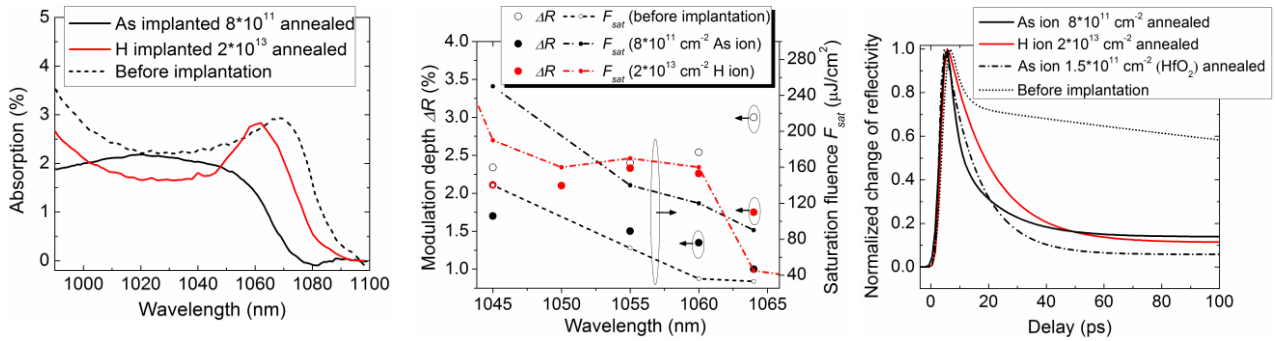

a) b) c)

Fig. 10. The influence of As ion (dose 8*10^{11} cm^{-2}) and H ion (dose 2*10^{13} cm^{-2}) implantation on the quantum well structure of anti-resonant SESAM: a) linear absorption spectra; b) nonlinear absorption spectra; c) pump-probe measurements at 1064 nm wavelength.

nonlinear modulation depth was comparable to the change of linear absorption (Fig. 10b). The reduction of SESAM relaxation times after the implantation and annealing measured at 1064 nm wavelength are shown in Fig. 10c. All SESAM were fast enough to mode-lock the fiber laser.

The As ion implanted resonant SESAM structure (τ_{rel} = 12 ps), with high modulation depth (ΔR = 3.7 %) and low saturation fluence (F_{sat} = 20 μJ/cm^2), was inserted into the resonator of fiber laser the dispersion of which was 14 ps/nm. The self-start mode-locking was achieved with a reliable operating window (~1.7). Depending on the coupling angle between the SESAM and optical fiber, it was possible to mode-lock at two different wavelengths (Fig. 11a). The broadest spectrum of a pulse was achieved at wavelength I which was measured to be τ_{PULSE} = 5.9 ps (Fig. 11b). Then, the accelerated damage test (see section 4) of the SESAM was performed in the nonlinear reflectivity measurement setup. The nonlinear reflectivity of SESAM was measured before and after ~3 hours of irradiation at the saturation parameter S = 110 (Fig. 11c). The measurements revealed no change in linear and nonlinear reflectivity parameters. This was different to the previous accelerated damage study of LT-grown resonant SESAM where a rapid (<2 h) drop of reflectivity was observed at the saturation parameter S = 108 (see Fig. 5c in section 4). Therefore, the high quality SESAM with a relatively small number of quantum

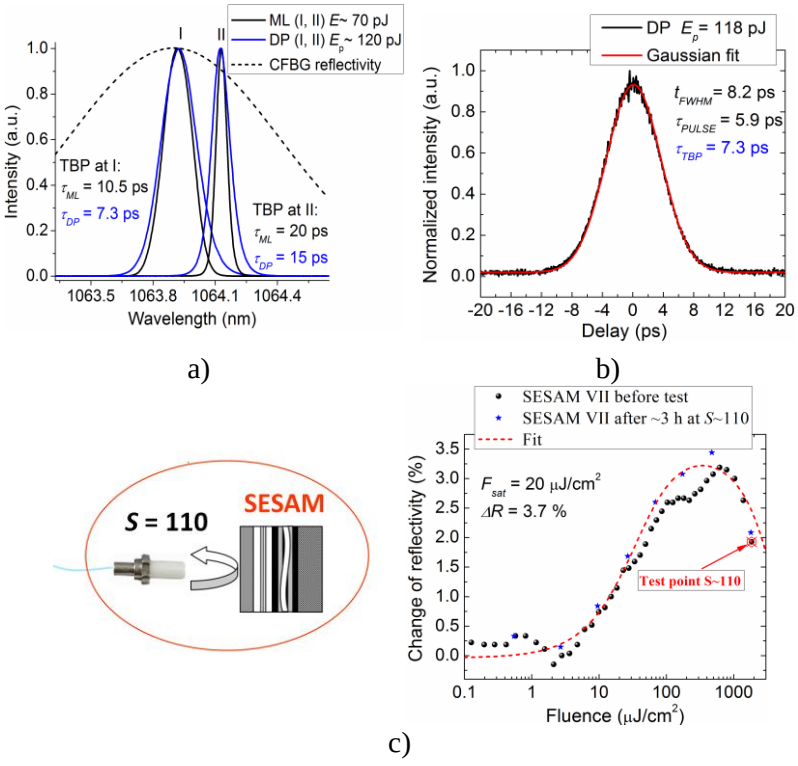

Fig. 11. a) The spectra of fiber laser which was mode-locked with the As ion implanted resonant SESAM; b) the autocorrelation trace at E_p = 118. c) The nonlinear reflectivity of As ion implanted resonant SESAM measured before and after an accelerated damage experiment at saturation parameter S = 110.

wells (n = 3) was suitable for the reliable operation of fiber laser. Although the excitonic absorption of quantum wells was modified after the implantation of heavy As ions, the saturation fluence remained sufficiently low and significantly decreased after the coating of resonant HfO_2 layer. The resistance of a quantum well structure to intense optical radiation was also improved.

Chapter 6. Single-wall carbon nanotubes for mode-locking of fiber laser

In this chapter, the nonlinear optical properties of semiconducting single-wall carbon nanotubes (SWCNTs) with two different diameters were investigated near the absorption maximum of excitonic feature. The first sample consisted of ~1.4 nm diameter nanotubes (produced by *Nanointegris*), the second one – of ~0.8 nm diameter SWCNTs (produced by *SouthWest Nano Technologies*).

The larger diameter SWCNTs (~1.4 nm) were dispersed using three different surfactants – sodium dodecyl sulphate (SDS, Fig. 12a), poly(4-vinylpyridine) (P4VP, Fig. 12b) and

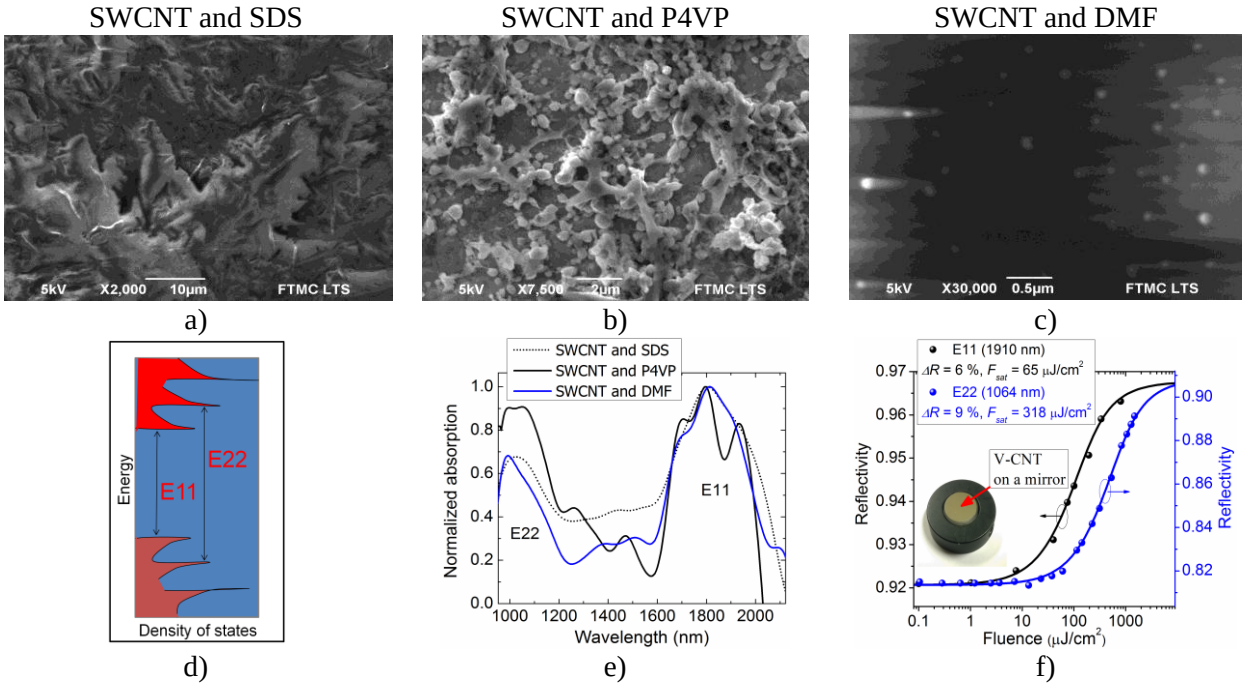

Fig. 12. Type I SWCNTs (~1.4 nm): a) SEM image of SDS assisted SWCNT dispersion; b) SEM image of P4VP assisted SWCNT dispersion; c) SEM image of DMF assisted SWCNT dispersion; d) principal diagram of first (E11) and second (E22) excitonic transitions; e) absorption spectra of SWCNTs with the E11 at around 1900 nm and E22 at around 1050 nm; f) The nonlinear reflectivity of SWCNTs, measured at 1910 nm (nat E11) and 1064 nm (at E22) wavelengths.

Dimethylformamide (DMF, Fig. 12c). These nanotubes had the first excitonic transition (E11) at around 1900 nm and second (E22) – at around 1050 nm (Fig. 12d and e). Although the nonlinear modulation depths of these transitions were comparable (Fig. 12f), the saturation fluence for the E22 transition (F_{sat}= 318 μJ/cm^2) was almost five times higher than of the E11 transition (F_{sat}= 65 μJ/cm^2).

The first excitonic transition of ~0.8 nm diameter SWCNTs was at around 1030 nm (Fig. 13a). This sample was also investigated in ~1 μm wavelength region. The main difference from type I nanotubes was of much lower saturation fluence (F_{sat}= 8 μJ/cm^2) for the E11 transition (Fig. 13b) compared to the E22 transition of ~1.4 nm SWNTS (F_{sat}= 329 μJ/cm^2).

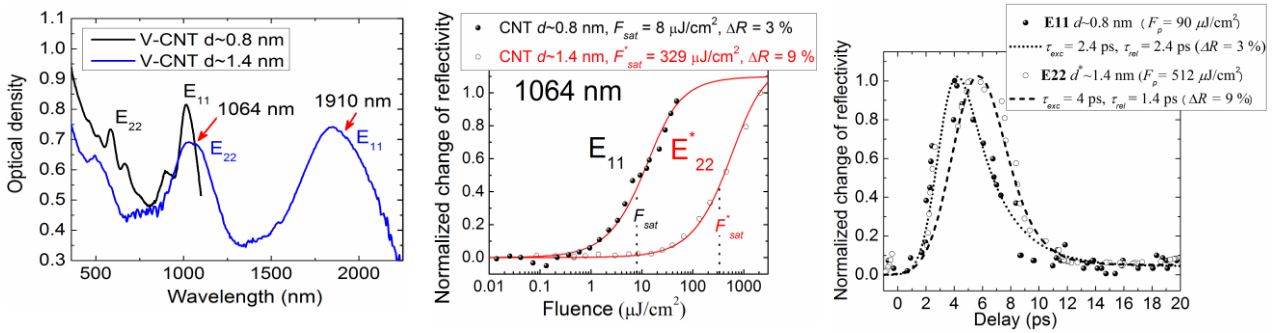

a) b) c)

Fig. 13 Type I (~1.4 nm) and type II (~0.8 nm) SWCNT saturable absorbers: a) the linear absorption spectra of SWCNTs; b) the nonlinear reflectivity, measured at 1064 nm wavelength; c) the pump-probe measurement, performed at the same 1064 nm wavelength.

Both samples possessed ultrafast carrier recovery time at 1064 nm wavelength (Fig. 13c) which was suitable for mode-locking of fiber laser.

The high saturation fluence of type I SWCNTs was the main limiting factor to mode-lock the fiber laser at ~1 μm wavelength, yet that was not the case for the ~2 μm wavelength region. This region is particularly important for medical application and the need for a fiber integrated device is very relevant. Accordingly, the new type of fiber integrated SWCNT saturable absorber was developed. The single-mode fiber was ablated by a femtosecond laser to produce the micro-groove (Fig. 14a). The width of the groove was chosen to be 18 μm, while the depth was adjusted by actively monitoring the insertion losses of SM fiber during the manufacturing process. Then, the grooves of different lengths were filled with the type I SWCNTs and the nonlinear transmission measurements were performed at 1064 nm wavelength (Fig. 14b). The main finding of these measurements was

the high nonlinear change of transmission. The lowest saturation fluence of the SWCNT device was for the longest micro-groove (5 mm) saturable absorber. However, the longest micro-groove had the highest linear losses.

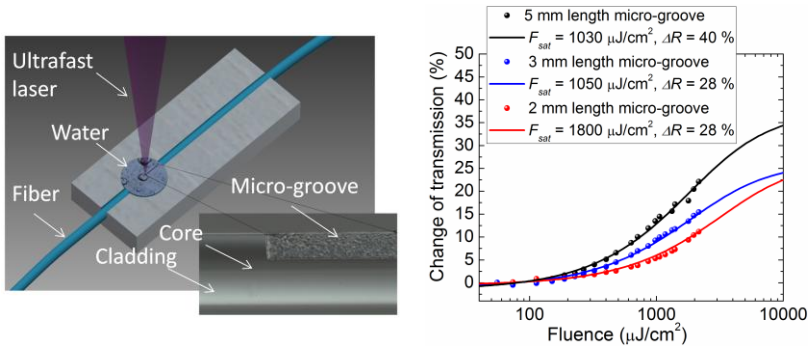

a) b)

Fig. 14. a) The schematic representation of micro-groove ablation in a single mode fiber. b) The change of nonlinear transmission measured at 1064 nm for the micro-grooves filled with type I SWCNTs.

To confirm the performance of the type I (~1.4 nm) SWCNT saturable absorbers, they were used to mode-lock the Tm/Ho fiber laser at ~2 μm wavelength (Fig. 15). This was done with both types of saturable absorbers – SWCNTs deposited on a silver mirror (M-CNT) and SWCNTs deposited into the micro-groove of an optical fiber (SM-CNT). Although the mode-locking was possible with both types of saturable absorbers, SM-CNT had higher mode-locking thresholds, indicating a higher saturation fluence of the device.

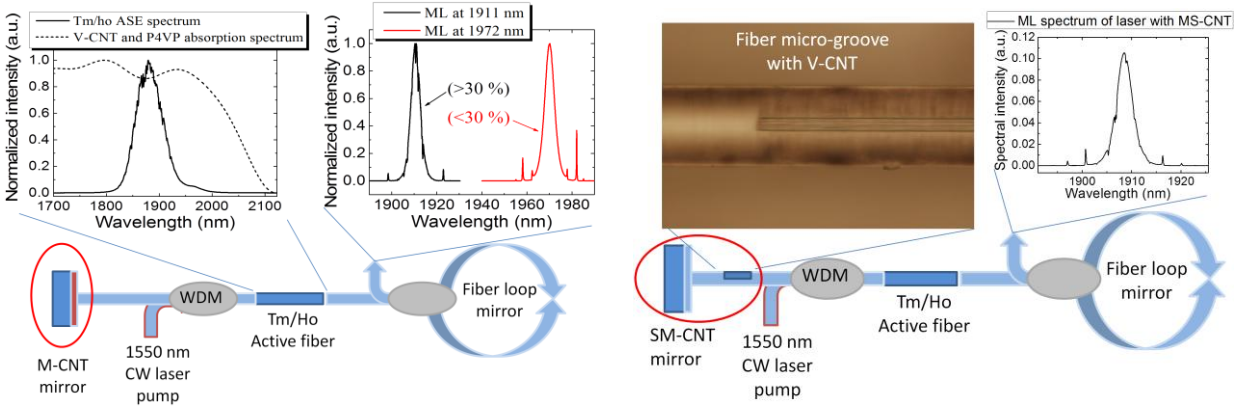

a) b)

Fig. 15. a) The schematic representation of picoseconds fiber oscillator which was mode-locked with type I (~1.4 nm) SWCNTs deposited on a silver mirror. The inset on the left shows the ASE spectrum of Tm/Ho doped fiber. The inset on the right shows two different pulse spectra measured at the oscillator output. b) The schematic representation of picoseconds fiber oscillator which was mode-locked with the large diameter (~1.4 nm) SWCNTs deposited into the micro-groove of single mode fiber. The inset on the left shows the optical microscope image of deposited fiber micro-grove. The inset on the right shows the pulse spectrum measured at the oscillator output.

Low saturation fluence of a saturable absorber is a very desirable parameter for ultrafast laser mode-locking [4]. Therefore, the type II (~0.8nm diameter) SWCNTs with low

saturation fluence (F_{sat}= 8 μJ/cm^2 at 1064 nm wavelength) were further investigated. The nonlinear reflectivity measurement of type II SWCNT mirror at different wavelengths (1020-1070 nm) revealed different nonlinear behavior of single-walled carbon nanotubes which consisted of two different chiralities [16] – (7,5) and (10,2) (Fig. 16a). It was found that the saturation fluence is low and almost constant (<10 μJ/cm^2) in the whole wavelength region, except at the intersection of spectral absorption lines of individual nanoparticles where it sharply rises to >100 μJ/cm^2. The measured diameter of different chirality nanotubes revealed close values [17]: ~0.82 nm for (7,5) and ~0.87 nm for (10,2). The absorption peaks of the individual nanotubes were impossible to resolve from conventional measurement of linear absorption spectra, but they were observed in the nonlinear reflectivity measurement of SWCNT absorber mirror at low fluence (<100 nJ/cm^2) (Fig. 16b). Finally, type II SWCNT mirror was used as a saturable absorber to mode-lock the picosecond fiber oscillator at 1064 nm wavelength. The oscillator's output spectra at single pulse and double pulse thresholds are shown in Fig. 16b. The easy self-starting operation with a sufficiently broad operating window (~1.8) verified the good potential of small diameter SWCNTs to use as a saturable absorber at 1 μm wavelength. However, the separation of different chirality individual carbon nanotubes is necessary in order to maintain the high nonlinearity of the E11 excitonic absorption at different wavelengths.

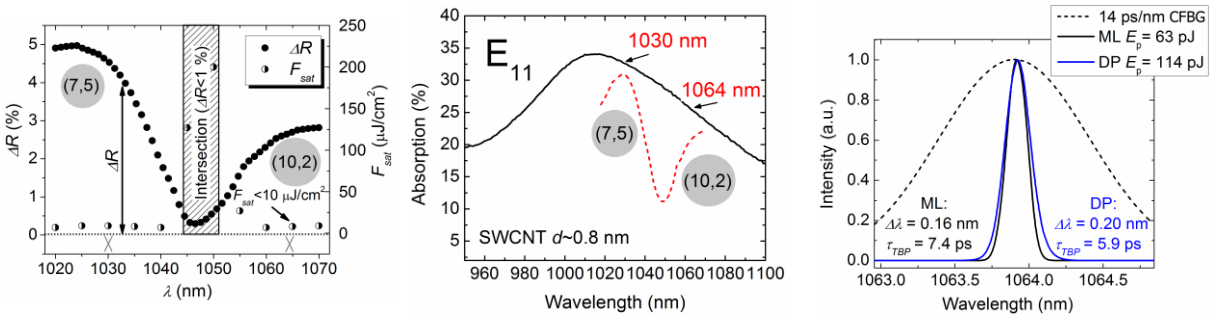

Fig. 16. Type II (~0.8 nm) SWCNT saturable absorber: a) the nonlinear modulation depth Δ*R* (left scale) and saturation fluence F_{sat} (right scale) measured at different wavelengths; b) the linear absorption spectra which were measured with conventional spectroscopy (solid curve) and nonlinear reflectivity setup (dashed line) where the spectral peaks at ~1030 nm and ~1064 nm indicate the absorption maxima of two individual species of SWCNTs; c) the pulse spectra measured at the oscillator (dispersion ~14 ps/nm) output near the mode-locking (black curve) and double pulse (blue curve) thresholds. Dashed line indicates the normalized reflectivity spectrum of CFBG.

Chapter 7. The nonlinear optical properties of PbSe quantum dot and silver nanoprism saturable absorbers

In this chapter, the PbSe quantum dot saturable absorber, which represents the lowest dimensionality (0D) structure, was investigated. Also, the silver nanoprism saturable absorber was introduced as a potentially new nanomaterial for fiber laser mode-locking applications.

The PbSe quantum dot doped phosphate glass sample was grown by the secondary heat treatment method [18]. The initial thickness of the sample of ~1 mm was polished to ~250 μm in order to minimize the nonsaturable absorption when focusing the light to a small diameter (~6.6 μm) spot. The linear absorption spectrum of the quantum dots is shown in Fig. 17a (solid black curve) together with the absorption spectrum (red curve) measured with the nonlinear reflectivity setup at low fluences (<100 nJ/cm^2) in the 1020-1074 nm spectral range. The excitonic absorption peak is at ~1064 nm for both absorption spectra. At this wavelength, the nonlinear reflectivity measurement revealed the F_{sat} = 11 μJ/cm^2 and ΔR = 3.3 % of PbSe quantum dot saturable absorber (Fig. 17b). For shorter wavelengths, the saturation fluence increased significantly from F_{sat} = 11 μJ/cm^2 at 1064 nm to F_{sat} = 125 μJ/cm^2 at 1020 nm (see Fig. 17a). This indicated the typical nonlinear optical properties at the excitonic feature of low dimensional saturable absorbers. The quantum dot sample possessed ultrafast carrier recovery time (~26 ps) at 1064 nm wavelength (Fig. 17c) which

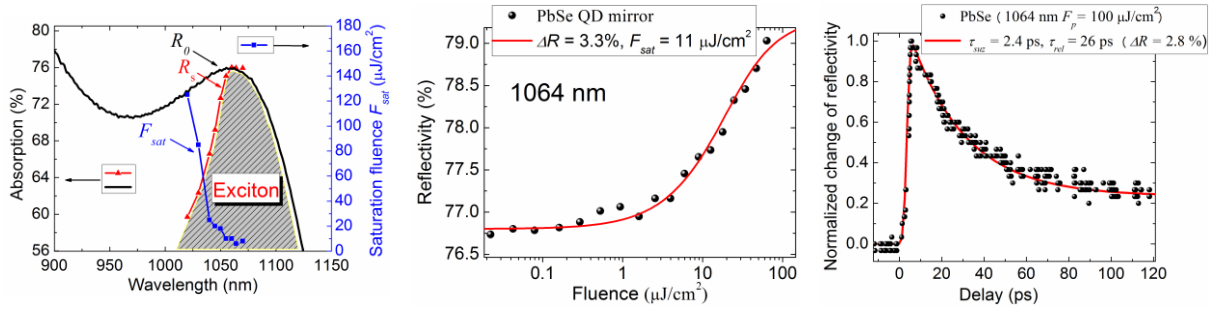

a) b) c)

Fig. 17. PbSe quantum dot saturable absorber: a) the linear absorption spectra of SWCNTs (left scale) measured with both the conventional spectrometer and nonlinear reflectivity setup. The blue curve represents the measured saturation fluence at different wavelengths (right scale); b) the nonlinear reflectivity, measured at 1064 nm wavelength; c) the pump-probe measurement, performed at the same 1064 nm wavelength.

was tolerable for mode-locking of fiber laser. However, the ration between nonsaturable losses and modulation depth was close to 10 and, together with low modulation depth (~3.3 %), was the main limiting factor to mode-locking the fiber laser. In order to achieve higher modulation depth of the PbSe quantum dot saturable absorber, the concentration of nanoparticles in a phosphate glass matrix must be increased, even though it is usually difficult to achieve [18].

Silver nanoprisms (Ag-NP) are also promising material for saturable absorbers. The suspension with Ag-NPs was prepared using the chemical synthesis method [19]. Then, the nanoparticles were mixed with organic polymer ORMOCER and samples of different thickness were prepared. The surface plasmon resonance was clearly seen in a linear absorption spectra of an Ag-NP ORMOCER sample and appeared as a broadened peak with a maximum at around 1064 nm wavelength (Fig. 18a). It was possible to enhance the absorption by increasing the concentration of Ag-NPs in an ORMOCER matrix. The nonlinear reflectivity measurements of an Ag-NP sample revealed two main nonlinear effects – self-focusing and saturable absorption. The surface plasmon resonance was the main mechanism of saturable absorption which is shown in Fig. 18b (red and blue curves), but the self-focusing was the reason of induced absorption. The saturable absorption was visible only when the incident beam was strongly defocused on the sample. Therefore, the saturation fluence of Ag-NPs was too high for mode-locking of fiber laser. The strong induced absorption at high fluencies (>1000 μJ/cm^2) was assigned to the free carrier

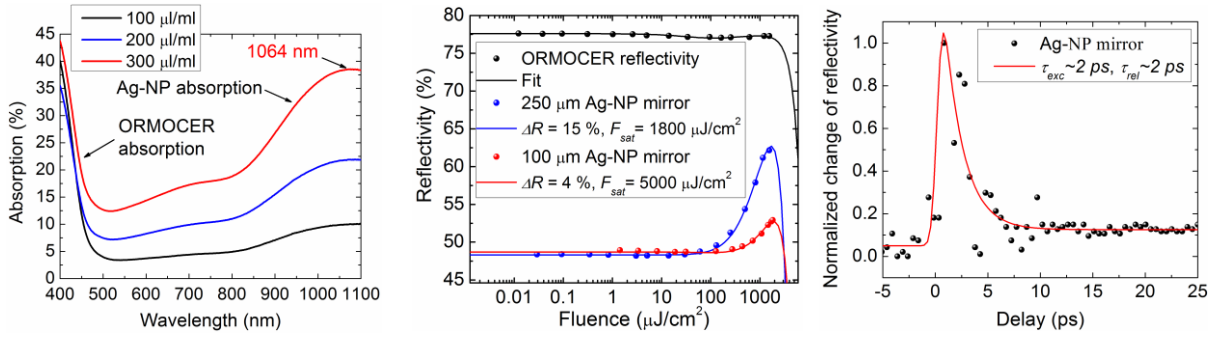

a) b) c)

Fig. 18. a) The linear absorption spectra of Ag-NP ORMOCER; b) the nonlinear reflectivity of both Ag-NP in ORMOCER (blue and red) and ORMOCER host alone (black) measured at 1064 nm wavelength; c) the pump-probe measurement of Ag-NP ORMOCER absorber, performed at the same 1064 nm wavelength.

absorption in an ORMOCER host. The pump probe measurement revealed the ultrafast carrier recovery of an Ag-NP absorber (~2 ps) at 1064 nm wavelength (Fig. 18c).

Conclusions

1. In order to mode-lock the fiber laser, it is necessary to use a SESAM with balanced modulation depth and low saturation fluence. Loss modulation must be large enough (>4 %) to initiate self-start mode-locking of a fiber laser, but should not exceed the limit value to prevent Q-switching instabilities. Low saturation fluence of a saturable absorber minimizes the requirement of high nonlinear modulation depth for initiating the self-start mode-locking.
2. It is possible to tune the pulse duration and energy of Yb-doped fiber laser by changing the amount of anomalous dispersion in a resonator. The dispersion of a fiber resonator and the nonlinear parameters of a saturable absorber also define the reliable operating window – pulse energy ranges between a single pulse and double regime. This operating window is largest for the highest anomalous dispersion value of a fiber resonator and the highest modulation depth of SESAM. The SESAM could be slow compared to the pulse duration, but should not exceed the maximum value of relaxation time which is about 20 times longer than the pulse duration.
3. For LT-grown high modulation depth (ΔR>20 %) SESAMs the thermally induced optical modification of InGaAs quantum well region was the most likely reason of long-term gradual degradation of the device at low incident energy fluencies (S<35). Also, the degradation of nonlinear parameters was faster for SESAMs with shorter relaxation; therefore, the damage process is related to the high number of defects in a quantum well region. This was verified with the pump-probe measurements where the relaxation time of SESAM receded after the long term exposure to an intense optical radiation. The instant critical optical damage (COD) of the SESAM occurs at the higher fluences (S>70) and is related to the two-photon absorption in the semiconductor layers outside the quantum well structure.

4. Despite the pulse energy, duration and repetition rate used for long-term optical degradation experiments, the modulation depth decreased to ~14-18 %, but the saturation fluence was affected much more differently. Therefore, the influence of irradiation parameters on the change of saturation fluence of the SESAM was studied in detail and showed almost linear growth of degradation speed with increasing of the average radiation intensity. Also, the optical degradation initiation threshold of a LT-grown high modulation depth InGaAs SESAM was measured to be ~200 μJ/cm^2. The SESAM which operated near this threshold in a resonator of low dispersion (1.6 ps/nm) fiber laser remained strongly unaffected, even after ~18 000 h of permanant operation.
5. The excitonic feature of a quantum well structure strongly influenced the nonlinear optical reflectivity parameters of a SESAM. The highest modulation depth ΔR and lowest saturation fluence F_{sat} were at the excitonic absorption maximum of the quantum well absorber. Measuring at shorter wavelengths, the saturation fluence sharply increases, but the modulation depth remains almost constant.
6. It is possible to reduce the excited carrier relaxation time of HT-grown InGaAs SESAM from ~390 ps to ~15 ps using both the heavy ion (As) and light ion (H) implantation techniques, but the modification of the structure is different. By using H ions, it was possible to implant them into a quantum well region of the SESAM structure using moderate energy, in turn creating only low energy point defects which can be easily annealed. However, in order to reach the same effective relaxation time of the SESAM, the implantation dose of H ions must be more than two orders of magnitude higher than for the As ions. The As ions create defects which influence both the excitation and relaxation times of the SESAM.
7. Although the modulation depth of a single-wall carbon nanotube saturable absorber at the first E11 and second E22 excitonic states are comparable, the saturation fluence of the second excitonic state is almost two orders of magnitude higher. In order to achieve a reliable self-start mode-locking of a fiber laser at ~2 μm or ~1 μm wavelengths, it is necessary to use single-wall carbon nanotubes which have first excitonic transition near the laser wavelength. However, for both the E11 and E22 states, the excited carrier

relaxation time is very fast (<3 ps) and is suitable for mode-locking of fiber lasers. Also, it is necessary to separate the SWCNTs of different diameters, as at the intersection of absorption spectra of corresponding chilarity nanotubes usually degrade the modulation depth and saturation fluence of a saturable absorber.

8. A single-wall carbon nanotube saturable absorber, fabricated in the micro-groove of a single mode optical fiber, is suitable for mode-locking of a fiber laser, but the saturation fluence was measured to be several times higher than for the carbon nanotube saturable absorber mirrors.
9. The saturation fluence of PbSe quantum dots near the first excitonic state is lower than in the InGaAs quantum well and is comparible to the single wall carbon nanotube saturable absorbers at ~1 μm wavelength, but the nonsaturable losses are very high compared to the nonlinear modulation depth. This is related to the intersection of the excitonic state with the continuum states. At this intersection, the modulation depth of PbSe quantum dot saturable absorber is only of few percent and could not be increased significantly.
10. The surface plasmon resonance was the main mechanism of saturable absorption in an Ag-NP ORMOCER sample, but the self-focusing was the reason of induced absorption. The saturable absorption was only visible when the beam was strongly defocused on the sample. Therefore, the saturation fluence of Ag-NP was too high for mode-locking of a fiber laser. The pump probe measurement revealed the ultrafast carrier recovery of an Ag-NP absorber (~2 ps) at 1064 nm wavelength.

References

[1] A. H. Zewail, “Femtochemistry. Past, present, and future,” *Pure Appl. Chem.*, vol. 72, no. 12, pp. 2219–2231, 2000.

[2] A. Stolow, A. E. Bragg, and D. M. Neumark, “Femtosecond time-resolved photoelectron spectroscopy,” *Chem. Rev.*, vol. 104, no. 4, pp. 1719–1757, 2004.

[3] M. E. Fermann, A. Galvanauskas, and G. Sucha, *Ultrafast lasers - Technology and Applications*. 2003.

[4] M. E. Fermann and I. Hartl, “Ultrafast fibre lasers,” *Nat. Photonics*, vol. 7, no. 11, pp. 868–874, 2013.

[5] F. Krausz, M. E. Fermann, T. Brabec, P. F. Curley, M. Hofer, M. H. Ober, C. Spielmann, E. Wintner, and A. J. Schmidt, “Femtosecond Solid-State Lasers,” *IEEE J. Quantum Electron.*, vol. 28, no. 10, pp. 2097–2122, 1992.

[6] M. Haiml, R. Grange, and U. Keller, “Optical characterization of semiconductor saturable absorbers,” *Appl. Phys. B*, vol. 79, pp. 331–339, 2004.
[7] R. Paschotta and U. Keller, “Passive mode locking with slow saturable absorbers,” *Appl. Phys. B Lasers Opt.*, vol. 73, no. 7, pp. 653–662, 2001.
[8] K. Viskontas, K. Regelskis, and N. Rusteika, “Slow and fast optical degradation of the SESAM for fiber laser mode-locking at 1 μm,” *Lith. J. Phys.*, vol. 54, no. 3, pp. 127–135, 2014.
[9] W. Jung, W. Benalcazar, A. Ahmad, U. Sharma, H. Tu, and S. a Boppart, “Numerical analysis of gradient index lens-based optical coherence tomography imaging probes.,” *J. Biomed. Opt.*, vol. 15, no. 6, p. 066027, 2010.
[10] O. Okhotnikov, A. Grudinin, and M. Pessa, “Ultra-fast fibre laser systems based on SESAM technology: New horizons and applications,” *New J. Phys.*, vol. 6, pp. 1–22, 2004.
[11] X. Liu, L. Qian, and F. Wise, “Generation of optical spatiotemporal solitons,” *Phys. Rev. Lett.*, vol. 82, no. 23, pp. 4631–4634, 1999.
[12] R. Paschotta, J. Nilsson, A. C. Tropper, and D. C. Hanna, “Ytterbium-doped fiber amplifiers,” *IEEE J. Quantum Electron.*, vol. 33, no. 7, pp. 1049–1056, 1997.
[13] S.-W. Ryu, I. Kim, B.-D. Choe, and W. G. Jeong, “The effect of strain on the interdiffusion in InGaAs/GaAs quantum wells,” *Appl. Phys. Lett.*, vol. 67, no. 1995, pp. 1417–1419, 1995.
[14] C. J. Saraceno, C. Schriber, M. Mangold, M. Hoffmann, O. H. Heckl, C. R. E. Baer, M. Golling, S. Thomas, and U. Keller, “SESAMs for high-power oscillators: design guidelines and damage thresholds,” vol. 18, no. 1, pp. 29–41, 2012.
[15] M. Josef Lederer, V. Kolev, B. Luther-Davies, H. Hoe Tan, and C. Jagadish, “Ion-implanted InGaAs single quantum well semiconductor saturable absorber mirrors for passive mode-locking,” *J. Phys. D Appl. Phys*, vol. 34, pp. 2455–2464, 2001.
[16] S. Ghosh, S. M. Bachilo, and R. B. Weisman, “Advanced sorting of single-walled carbon nanotubes by nonlinear density-gradient ultracentrifugation,” *Nat. Nanotechnol.*, vol. 5, no. 6, pp. 443–450, 2010.
[17] T. G. Pedersen, “Exciton effects in carbon nanotubes,” in *Carbon*, 2004, vol. 42, no. 5–6, pp. 1007–1010.
[18] a. Lipovskii, E. Kolobkova, V. Petrikov, I. Kang, a. Olkhovets, T. Krauss, M. Thomas, J. Silcox, F. Wise, Q. Shen, and S. Kycia, “Synthesis and characterization of PbSe quantum dots in phosphate glass,” *Appl. Phys. Lett.*, vol. 71, no. 23, p. 3406, 1997.
[19] A. Alesenkov, J. Pilipavičius, A. Beganskienė, R. Sirutkaitis, and V. Sirutkaitis, “Nonlinear Properties of Silver Nanoparticles Explored By a Femtosecond Z-Scan Technique,” vol. 55, no. 2, pp. 100–109, 2015.

CURRICULUM VITAE

Name, Surname:	**Karolis Viskontas**
Date of birth and place:	**1982 05 08**, Vilnius, Lithuania
Education:	**2000** "Gerosios vilties" secondary school, Vilnius
	2004 Bachelor Degree, Physics, Vilnius University
	2006 Master Degree, Physics, Vilnius University
	2011-2016 PhD studies, Center for Physical Sciences and Technology, Vilnius, Lithuania

Santrauka

Šio darbo tikslas buvo pritaikyti skirtingų nanostruktūrinių medžiagų įsisotinančius sugėriklius skaidulinių lazerių modų sinchronizavimui, nustatyti optimalius įsisotinančio sugėriklio parametrus tokio tipo skirtingų konfigūracijų lazeriams, bei pagaminti, ištirti ir integruoti tinkamiausių parametrų įsisotinantį sugėriklį į skaidulinio lazerio rezonatorių.

Buvo sukurta unikali visiškai skaidulinė netiesinio atspindžio ir žadinimo-zondavimo matavimo sistema su derinamu lazeriniu šaltiniu. Todėl, pirmą kartą buvo atlikti ilgalaikiai (>4000 h) SESAM tipo sugėriklių patikimumo matavimai itin trumpų impulsų lazerio rezonatoriuje. Ilgalaikiai matavimai buvo palyginti su pagreitintais matavimais ir nustatyta, kad pažeidimo mechanizmas skirtingas, todėl negalima vertinti įsisotinančio sugėriklio ilgaamžiškumą pagal kritinio optinio pažeidimo slenkstį. Sukurtos optimalios schemos, siekiant užtikrinti patikimą ir ilgaamžį (>18 000h) itin trumpų impulsų (<10 ps) skaidulinio lazerio veikimą.

Parodyta, kad dirbti ties pirmąją eksitonine juosta yra būtina sąlyga bet kokio dimensiškumo medžiagoms, norint turėti didžiausio netiesinio nuostolių moduliacijos gylio ir mažiausio įsotinimo srauto sugėriklį, tinkantį skaidulinių lazerių išilginių rezonatoriaus modų sinchronizavimui. Pademonstruota, kad mažinant puslaidininkio dimensiškumą galima pasiekti vis mažesnį įsotinimo srautą ~1 μm bangos ilgių srityje, pradedant nuo SESAM (2D) ir baigiant PbSe kvantiniais taškais (0D). Nustatyta, kad be įsotinimo srauto, kiti nanostruktūrinių medžiagų įsisotinančio sugėriklio parametrai labai priklauso nuo pasirinktos gamybos technologijos, struktūros matmenų bei atominių medžiagos savybių.

Taip pat, šis darbas turėjo praktinę vertę pritaikant itin trumpų impulsų skaidulinių lazerių technologiją komerciniais tikslais ir vystant šią technologiją Lietuvoje. Atlikti tyrimai gali būti pritaikyti naujų patikimų įsisotinančių sugėriklių ar netiesinių optinių komponentų gamybos technologijos sukūrimui.